Plant, Cell & Environment

WILEY

Plant, Cell & Environment

ORIGINAL ARTICLE OPEN ACCESS

Dasineura asteriae Reprograms the Flower Gene Expressions of Vegetative Organs to Create Flower-Like Gall in *Aster scaber*

Kyung-Hwan Boo[1,2] | Young Kyoung Oh[3] | Christian Møller[3] | Doseung Lee[4] | Gyeong Lyong Jeon[1] | Donghyuk Kim[5] | Meike Burow[6] | Dominik Kilian Großkinsky[6,7] | Jiwon Kim[1,2] | Moon Young Ryu[8] | Bora Lee[8] | Jiye Suh[9] | Chan Man Ha[10] | Thomas Roitsch[6,11] | Pyung Ok Lim[12] | Frederic Berger[13] | Joo-Won Suh[14] | Soon-Il Kim[15] | Tae Rin Oh[16] | Seok Keun Cho[8] | Wanggyu Kim[17] | Sangtae Kim[9] | Key Zung Riu[1,2] | Seong Wook Yang[3]

[1]Department of Biotechnology, College of Applied Life Sciences (SARI) Jeju National University, Jeju, South Korea | [2]Subtropical/Tropical Organism Gene Bank, Jeju National University, Jeju, South Korea | [3]Department of Systems Biology, College of Life Science and Biotechnology, Yonsei University, Seoul, South Korea | [4]Institute of Health and Environment, Jeju, South Korea | [5]School of Energy and Chemical Engineering, UNIST, UNIST-gil 50, Ulsan, South Korea | [6]Department of Plant and Environmental Sciences, Faculty of Science, University of Copenhagen, Copenhagen, Denmark | [7]AIT Austrian Institute of Technology, Center for Health & Bioresources, Bioresources Unit, Donau, Austria | [8]Xenohelix Research Institute, Incheon, South Korea | [9]Department of Biotechnology, Sungshin University, Seoul, South Korea | [10]Department of Biological Sciences, college of Arts and Sciences, University of North Texas, Denton, Texas, USA | [11]Department of Adaptive Biotechnologies, Global Change Research Institute, CAS, Brno, Czech Republic | [12]Department of New Biology, DGIST, Daegu, South Korea | [13]Gregor Mendel Institute of Molecular Plant Biology GmbH, Vienna, Austria | [14]Center for Nutraceutical and Pharmaceutical Materials, Department of Bioscience and Bioinformatics, Myongji University, Yongin, South Korea | [15]Institute of Research and Development, Nareso Co., Ltd., Seoul National University Business Incubator, Suwon, South Korea | [16]Department of Biochemistry and Biophysics, Texas A&M University, College Station, Texas, USA | [17]National Institute of Biological Resources, Environmental Research Complex, Incheon, South Korea

Correspondence: Sangtae Kim (amborella@sungshin.ac.kr) | Key Zung Riu (kzriu@jejunu.ac.kr) | Seong Wook Yang (yangsw@yonsei.ac.kr)

Received: 8 April 2025 | **Revised:** 5 August 2025 | **Accepted:** 6 August 2025

Funding: This study was supported by the National Research Foundation of Korea (NRF) grant funded by the Korean Ministry of Science and ICT (No. 2017R1A2B4010255) and by Samsung Science and Technology Foundation Project SSTF-BA1801-09 to S.W.Y. and was also supported by the Basic Science Research Program of the NRF funded by the Korean Ministry of Education (2016R1A6A1A03012862) and (2017R1D1A1B03034952) to K.Z.R and S.K., respectively. The "Cooperative Research Program for Agriculture Science & Technology Development (Project No. PJ01319101)" funded by the Korean Rural Development Administration and a grant (715003-07) from the Research Center for Production Management and Technical Development for High Quality Livestock Products through Agriculture, Food and Rural Affairs Research Center Support Program, Ministry of Agriculture, Food and Rural Affairs to K.Z.R. Lastly, this study was supported by the National Sustainability Program I (NPU w, grant number LO1415) funded by the Ministry of Education, Youth, and Sports of the Czech Republic to T.R. F.B. was supported by core funding from GMI.

Keywords: floral reprogramming | insect-induced plant gall | plant-insect interaction | redifferentiation

ABSTRACT

Plant galls are abnormal growing tissues induced by various parasitic organisms, exhibiting diverse and complex morphologies. Typically, these galls differ significantly in appearance from their host plants. Here, we report that larvae of a parasitic fly generate unique, rosette galls on *Aster scaber*, a perennial herb. These galls develop from vegetative organs after the larvae reprogram floral gene expression. To investigate the underlying mechanisms, we conducted whole-genome sequencing and transcriptome analysis. Our findings reveal that the larvae induce host organ dedifferentiation into an amorphous callus, activate floral genes, and selectively suppress genes associated with carpel development. As a result, the pseudoflowers consist

Kyung-Hwan Boo, Young Kyoung Oh and Christian Møller equally contributed to this study.

solely of tepal-like leaflets and a specialized chamber, and the larvae influence pigment biosynthesis. Hijacking plants developmental gene networks by insects to sequentially mediate dedifferentiation, cytokinin regulation, and tepal-like leaflets formation provides a framework to study highly elaborate forms of parasitism and symbiosis between plants and insects.

1 | Introduction

The earliest fossil records of galling extend back at least 300 million years ago, long before flowering plants emerged (Labandeira and Phillips 1996), and galling has repeatedly evolved in many insect orders (Stone and Schönrogge 2003). Today, a variety of insect galls can be induced by over 13 000 insect species worldwide (Espírito-Santo and Fernandes 2007), including aphids, plant lice, gall midges, gall flies, and gall wasps (Hardy and Cook 2010). Insect-induced galls vary widely in color, shape, and structural complexity (Oliveira et al. 2016). Although the simplest galls look like tissue deformities, complex galls have intricate internal and/or external structures. Many studies have discussed the adaptive significance of galling traits for nutrition enhancement, microenvironment creation, and enemy escape (Price et al. 1987; Stone and Schönrogge 2003) with the diversity and complexity of gall morphology. To elucidate the formation of complex gall structures and alterations in host defense and metabolism, many studies have analyzed the genes and proteins of insects and host plants (Bailey et al. 2015; Chen et al. 2008; Korgaonkar et al. 2021; Liu et al. 2013; Nabity et al. 2013; Oates et al. 2016; Sinha et al. 2012; Stern and Han 2022; Zhao et al. 2015; Zhao et al. 2016).

Several examples illustrate the complexity of insect-induced galls. Rhus galls, induced by aphids, are involved in tannin gene expressions (Chen et al. 2018). A galling parasite, *Daktulosphaira vitifoliae*, controls reproductive genes in wild grapevine (Schultz et al. 2019). A new galling weevil, *Smicronyx madaranus* enhances photosynthesis to form spherical galls on *Cuscuta campestris* (Murakami et al. 2021). The aphid *Schlechtendalia chinensis* forms horned galls on *Rhus chinensis*, with active nutrient recycling and CO_2 exchange (Chen et al. 2020). Genome sequencing of the aphid *S. chinensis* identified genes linked to gall formation and plant defense suppression, providing insight of insect-plant interactions (Wei et al. 2022). In *Zizania latifolia*, short-day conditions promote gall swelling and are linked to seasonal cues via the CONSTANS-FLOWERING LOCUS T pathway (Zhang et al. 2024). Profiling of oak galls has identified distinct biochemical pathways and hormone signaling shaping gall morphology (Markel et al. 2024). Microbial contributions to gall formation have been suggested, as in *Iatrophobia brasiliensis*, which uses bacteria to genetically transform cassava (Gätjens-Boniche et al. 2023), though consistent microbial involvement remains unconfirmed (Hammer et al. 2021). Some interactions, like *Hormaphis cornu* secreting the DGC protein to trigger anthocyanin biosynthesis in Witch-hazel cone galls, provide rare molecular insight into how insect-derived factors may influence host development (Korgaonkar et al. 2021). However, such mechanisms remain largely unknown.

In this study, we describe an insect gall formed on *Aster scaber* (*A. scaber*) that resembles a primitive floral structure of the Asteraceae family. Previous studies reported that at least five different types of insect galls occur on the organs of *A. scaber* in Korea and Japan (Paik et al. 2004; Tokuda et al. 2003). However, the galler for the sub-globular galls that we found on the host flower was not identified. From the hundreds of insects visiting *A. scaber* in our study site, we identified that it was the larva of *Dasineura asteriae* (*D. asteriae*) (Paik et al. 2004) that induced the galls. Although *D. asteriae* was classified as a gall-forming fly (Shinji 1944), its life cycle has not been elucidated. To identify the genes involved in this process, we performed whole genome sequencing, assembling the 4.92 GB genome of *A. scaber*. Additionally, we conducted transcriptome analysis *in silico* and *in planta* to characterize the insect-regulated gene expressions in *A. scaber*. We also observe phenotypic changes using scanning electron microscopy (SEM). Together, our study elucidates a developmental pathway leading to flower-like gall formation.

2 | Materials and Methods

2.1 | Gall Observation and Collection Sites

Over the past two decades, we have collected a great number of unique plant galls that emerge specifically on a perennial herb, *A. scaber* (Asteraceae; Compositae), on Mt. Halla (1952 m above sea level), Jeju Province, a subtropical island at the south end of Korea (Yukawa et al. 2014). *A. scaber* is also called *Doellingeria scabra* (Thunb.) Nees, after the circumscription of *Aster* was narrowed (Nesom 1994). We use *A. scaber* in this paper based on recent molecular analysis (Li et al. 2012).

Galls on *A. scaber* were found in deciduous forest and grass fields at 300–530 m above sea level. *A. scaber* samples used in this study were collected at four sampling sites located at 33° 25′ 47″ N, 126° 33′ 22″ E; 33° 26′ 13″ N, 126° 34′ 04″ E; 33° 27′ 09″ N, 126° 44′ 12″ E; and 33° 22′ 01″ N, 126° 22′ 11″ E. *A. scaber* plants collected from the field were transplanted into pots or the ground in a greenhouse. The plants were grown without any pesticides to protect the larvae inside the galls. Gall photographs were taken with a digital camera (Cannon EOS 20D). Galls were categorized into these stages based on their diameter: early stage (approximately 7 mm), middle stage (approximately 10 mm), and late stage (greater than 10 mm). Leaves that did not have galls were used as a control leaf for analysis.

2.2 | Insect Identification

Adult female specimens of *D. asteriae* (Shinji) (Diptera; Cecidomyiidae) were collected in May from the nontransparent paper box in which larvae were reared and preserved in 70% ethanol solution for identification. The insect was identified by Dr. Makoto Tokuda, Kysuhu University, Japan.

2.3 | Microscopic Analysis

Insects in each developmental stage (egg, larva, pupa, and adult) were observed with the unaided eye or under stereomicroscope (Olympus SZX-ILLB100, JAPAN). Galls were sectioned in 70-μm-thick sections using a Vibratome Series 1000 (USA) to observe larvae and larval chambers. Sectioned samples were mounted on slide glass and observed under inverted-microscope (Olympus BX 60-F3, JAPAN). Galls for SEM and histological analyses were fixed overnight at room temperature in a solution of 50% ethanol, 5% glacial acetic acid, and 3.7% (v/v) formaldehyde. Samples were then dehydrated by sequential 30 min incubations in 50%, 60%, 70%, 80%, 90%, 95%, and 99.5% (v/v) ethanol, followed by two 1 h incubations in 100% (v/v) ethanol. Dehydrated samples were set in Technovit 7100 resin (Heraeus Kulzer, Wehrheim/Ts., Germany) at room temperature, once in 50% (v/v) resin and twice in 100% resin. For SEM analysis, samples were then critical point dried in liquid CO_2, coated with 10–20 μM thick gold and palladium, and imaged using SEM (Hitachi, Japan) at an acceleration voltage of 10–20 kV. For histological analysis, serial 3–4 μM thick sections of the samples were cut with a rotary microtome (Microm International, Germany), and stained with 0.5% Toluidine Blue for 30 s. Photographs were taken with an Axiovert inverted microscope (Carl Zeiss, Germany).

2.4 | DNA Sequencing, Genome Assembly and Annotation

For whole genome sequencing, samples were collected at various growth stages describe above accordingly and immediately ground in liquid nitrogen. For genomic DNA (gDNA) extraction, the ground tissue was treated with pre-warmed CTAB buffer (at 65°C) containing RNase and incubated at 65°C for 10 min. For purification, one-third of the volume of chloroform was added to the mixture, which was then gently inverted to mix. After centrifugation at 13 000 rpm for 5 min at room temperature to separate the phases, the upper aqueous phase was transferred to a new tube, and one-third of the volume of chloroform was added again to further purify the sample. For precipitation, an equal volume of isopropanol was added, and the solution was mixed gently before centrifugation. The gDNA pellet was washed with 70% ethanol after discarding the supernatant and then air-dried to remove residual ethanol. The dried pellet was dissolved in DEPC-treated water. The quality and quantity of the genomic DNA were assessed by electrophoresis and with a Nanodrop spectrophotometer.

For ONT-sequencing, two libraries were sequenced on a ONT-PromethION 24 with FLO-PRO002 flow cells, and basecalled with Guppy v.3.2.10. This resulted in 367 Gb of long-read data. A total of 770 Gb, 150 bp paired-end Illumina data was sequenced on an Illumina Nova-Seq platform. To estimate the genome size, a 21-mer spectrum was made from the filtered Illumina reads using KMC v.3.1.1 (Kokot et al. 2017) and GenomeScope2.0 (Ranallo-Benavidez et al. 2020). ONT-reads had adapters removed with PoreChop (https://github.com/rrwick/Porechop) and > 5 kb reads were assembled into contigs by SMARTdenovo (Liu et al. 2021). This assembly was first polished with the ONT-reads, using medaka followed by two rounds of short-read polishing by NextPolish (Hu et al. 2020). Haplotigs were removed using purge-haplotigs v.1.1.1 (Roach et al. 2018). Repetitive elements were detected with RepeatModeler v.2.0.2 and RepeatMasker v.4.1.2-p1 (Flynn et al. 2020). Protein-coding genes were predicted with GeMoMa v.1.7.1 (Keilwagen et al. 2019) using the six uninfected *A. scaber* RNA-seq libraries and homologous protein evidence from *Helianthus annuus* (Hannuus_494_r1.2), *Lactuca sativa* (Lsativa_467_v5) and *Cynara cardunculus* (GCA_001531365.1). Both the assembled genome, transcriptome and gene annotation were analyzed for the presence of BUSCO genes of the embryophyta_odb10 lineage by Compleasm v.0.2.6 (Huang and Li 2023).

2.5 | RNA-Sequencing and Analysis

High-quality total RNA was purified with XENOPURE Total RNA Purification kit (Xenohelix, South Korea). Poly(A) RNA was isolated from 1 to 10 μg of high-quality total RNA and fragmented by Mg^{2+} ions into small pieces of mRNA. Double-stranded cDNA was then synthesized using the SuperScript Double-Stranded cDNA Synthesis kit (Invitrogen, USA) with random hexamer primers (Illumina, USA). cDNA were subjected to end-repair and phosphorylation using T4 DNA polymerase, Klenow DNA polymerase, and T4 polynucleotide kinase. The cDNA fragments were adenylated at the 3′ end with Klenow Fragment (3′→5′ exo). Paired-end adapters were attached to the ends of cDNA fragments, and these cDNA fragments were amplified by PCR with two primers that anneal to the ends of the adaptors. To select a size range of templates for downstream enrichment, the products of amplified cDNA fragments were run on an agarose gel, and 300–400-bp fragments were purified from the gel. Finally, the quality of our cDNA library was validated using Bioanalyzer (Agilent, USA). The cDNA library was loaded onto paired-end flow cells following Illumina's standard protocol by using the Illumina cBot paired-end cluster kit. The flow cell was sequenced on an Illumina HiSeq. 2000 sequencing system using the SBS (sequencing by synthesis) kit and HCS (HiSeq control software) data-collection software. Base calling was performed using Illumina's RTA (real-time analyzer) software.

Six tissues from a noninfected plant were sequenced, generating a minimum of 50 M reads per library. Reads were trimmed and filtered with Trimmomatic (http://www.usadellab.org/cms/?page=trimmomatic). The *A. scaber* reference transcriptome was assembled from the six wild-type RNA-seq libraries, using Trinity v.2.11.0 (full-length transcriptome assembly from RNA-seq data (Grabherr et al. 2011). The initial assembly of 397,722 transcripts was filtered by expression (TPM > 1.5) highly redundant transcripts were clustered together by cd-hit est v.4.8.1. Coding sequences were predicted with TransDecoder v.5.5.0 (https://github.com/TransDecoder/TransDecoder). Several flowering-related gene sequences were manually corrected.

For gene expression analysis of the gall, we did RNA-seq for pairs of gall/mother leaf, across the early, middle and late gall developmental stage. We used salmon in pseudo-alignment

mode to quantify gene expression, and the TMM method to normalize expression values (Patro et al. 2017). For heatmaps, log2 fold-change values were used, with a pseudocount of 0.1. Clustering was done by the pheatmap package in R.

2.6 | Comparative Genomics

The proteomes of five species, *A. scaber*, *Arabidopsis thaliana, C. cardunculus, H. annuus* and *Chrysanthemum morifolium* were clustered with OrthoFinder v.2.5.5. To draw gene trees, we aligned protein sequences of each orthogroup with MUSCLE and built the tree in MEGA-X using the maximum-likelihood method. The robustness of each node was estimated by the bootstrap method with 200 bootstraps.

2.7 | Probe Preparation for In Situ Hybridization

Based on RNA sequencing and analysis data, antisense sequences were selected as probe sequences for the gene of interest. Sense sequences were used as negative controls for each gene. The designed probe sequences are listed in Supporting Information: Table S1. Probe sequences were cloned into the pGEM-T Easy vector (Promega, USA), and in vitro transcription was performed using both T7 and SP6 RNA polymerases. Following in vitro transcription, probes were labeled with a DIG-RNA labeling kit (Roche, Switzerland). DNA was removed by DNase treatment, and probes were incubated at 60°C for 30 min to hydrolyze them into fragments of approximately 150 bp.

2.8 | In Situ Hybridization

For fixation, samples were treated with FAA solution [5% (v/v) formaldehyde, 5% (v/v) acetic acid, and 50% (v/v) ethanol; all from Merck, Germany]. Dehydration was performed using a graded series of ethanol and tert-butyl alcohol (Merck, Germany), followed by paraffin embedding using paraplast (Merck, Germany) and embedding molds (Simport, Canada). Paraffin blocks were stored at 4°C and sectioned at 10 μm thickness using an RM2245 microtome (Leica Biosystems, Germany). Deparaffinization was carried out with xylene (Merck, Germany), followed by ethanol washes and rehydration through graded ethanol solutions. Rehydrated sections were fixed with 4% (v/v) paraformaldehyde (Merck, Germany), rinsed with sterilized water, and acetylated using acetylation buffer (0.65% acetic acid and 1.3% triethanolamine). After a second dehydration step, sections were air-dried. For hybridization, DIG-labeled probes were applied in hybridization buffer containing 20 × SSC, 10×NTE, 10×DIG1, and 1×DIG3. Hybridization was performed overnight at 50°C in a humidified chamber. Post-hybridization, slides were washed with 4 × SSC, treated with RNase in pre-warmed 1×NTE at 30°C, and sequentially washed with 0.5 × SSC and DIG1 buffer. Signal detection was performed by applying chromogenic substrate and incubating slides in the dark for 4 h. Hybridization signals were visualized using a Dino-Lite digital microscope (AnMo Electronics Corporation, Taiwan).

2.9 | Transcripts Analysis

For Transcripts Analaysis, Real-time qPCR and droplet digital PCR (dd-PCR) Analysis were used. Samples were collected depending on their growth stage; early stage, middle stage and late stage for *A. scaber*. For comparison, *C. morifolium* were selected and collected depending on their tissues; three different stages of disc flowers and two different stages of ray flower, bract and leaf. All samples were ground with liquid nitrogen and used for total RNA extraction. Total RNA was extracted using XENOPURE Total RNA Purification kit (Xenohelix, South Korea). 1 μg of RNA was used for cDNA synthesis using Xeno cDNA Synthesis kit (Xenohelix, South Korea). For Real-time qPCR, synthesized cDNA was used as a template and reactions were performed using TB Green Premix Ex Taq TM II (Takara, Japan). Primers were designed in Primer3 and are listed in the supplementary data (Supporting Information S1: Table S2–S4). Amplification and analysis were performed RT-qPCR machine (Takara, Japan). Relative transcript levels were calculated based on *AsUBQ10 or CmEF1a* gene expression. Since no prior studies had established a housekeeping gene in this organism, we selected *AsUBQ10 or CmEF1a* based on RNA-seq data, identifying it as one of the most stably expressed genes across all samples. To further confirm its suitability, we performed qRT-PCR and observed minimal Ct value variation across experimental conditions. All expression analyses were performed in three independent replicates. Fold changes of transcripts and standard error were calculated with the $2^{-\Delta\Delta CT}$ analysis method.

For droplet digital PCR analysis, Qx200 Droplet Digital PCR System (Bio-rad, USA) were used according to the manufacturer's instruction. *AsUBQ10* was used for an internal control gene for checking the sample status. For comparison analysis, graphs were generated based on relative transcript levels, normalized to expression in leaf tissue.

2.10 | Phytohormone Analysis

Phytohormones were extracted from around 200 mg (fresh weight) of *A. scaber* sample mentioned above accordingly which ground in liquid nitrogen with 1.25 ml 80% (v/v) methanol containing 4 μL of internal standard (IS) mix (5 μg mL^{-1} in 80% methanol) composed of deuterium-labeled hormones (Großkinsky et al. 2014). Samples were thoroughly vortexed, incubated for 30 min at 4°C, and centrifuged (20.000 × *g*, 4°C, 15 min). Supernatants were passed through Chromafix C18 columns (Macherey-Nagel, Düren/Germany) after pre-equilibration with 3 mL 80% methanol and filtrates were collected in 5 mL tubes on ice. The extraction was repeated with 1.25 mL 80% methanol and second extracts were passed through the same columns. The combined extracts were concentrated using SpeedVac. The residues were dissolved in 1 mL 20% methanol by sonication for 8 min and passed through 0.2 μM syringe filters. The phytohormones were then analyzed by UHPLC/TQ-MS on an AdvanceTM-UHPLC/EVOQTMElite-TQ-MS instrument (Bruker) equipped with a C18 reversed phase column (Kinetex 1.7 u XB-C18, 10 cm × 2.1 mm, 1.7 μM particle size, Phenomenex) using a 0.05% (v/v) formic acid in water, pH 4.0 (solvent A) – methanol (solvent B) gradient at a flow rate of 0.4 mL/min at 40°C. The solvent B gradient applied

was as follows: 10%–50% (15 min), 50% (2 min), 50%–100% (0.1 min), 100% (2.9 min), 100%–10% (0.1 min), and 10% (5 min). Compounds were ionized by ESI with a spray voltage of +4500 V and −4000 V in positive and negative mode, respectively, heated probe temperature of 350°C, and cone temperature of 300°C. The individual hormones were monitored based on the following MRM transitions: ABA, (−) 263 > 153 [7 V]; cZ/tZ, (+) 220 > 136 [15 V]; IAA, (+) 176 > 130 [10 V]; JA, (−) 209 > 59 [11 V]; JA-Ile, (−) 322 > 130 [17 V]; SA, (−) 137 > 93 [20 V]; tZ7G/tZ9G/tZOG, (+) 382 > 220 [17 V]; tZR, (+) 352 > 220 [15 V]; tZROG, (+) 514 > 382 [15 V]. tZ7G, tZ9G, and tZOG as well as cZ and tZ were distinguished based on retention times compared to those of known standards.

2.11 | Statistical Analysis

For statistical analysis, data were analyzed using GraphPad Prism 8 software (GraphPad Software, San Diego, CA, USA). The quantitative data analysis was made based on three independent experiments representing mean ± standard deviation (SD). In each figure, specific tests and their statistical significance are indicated.

3 | Results

3.1 | Insect-Induced Rosette Galls in *A. scaber*

A. scaber grows up to around 1.2 m, blooms white hermaphrodite composite flowers during summer, and its seeds ripen around fall (Figure 1A). The galls observed on *A. scaber* are systemically arranged and display diverse colors such as yellow, pink, red, and white (Figure 1B,C; Supporting Information S1: Figure S1A). However, the morphology of the galls differs from that of the host flowers and is closer to the shape of water lily flower (Figure 1B,C; Supporting Information S1: Figure S1B). The host produces an inflorescence consisting of a cluster of disc flowers and ray flowers. In contrast, the rosette galls comprise larger numbers of tepal-like leaflets (Figure 1B,C; Supporting Information S1: Figure S1A). Regardless of morphological type, the fully matured rosette galls had 7 to 9 whorls, and each whorl had mainly three or five leaflets (Supporting Information S1: Figure S1A).

The galls formed on leaves, stems, and exposed roots and eventually colonized almost all *A. scaber* plants (Figure 1D). An anatomical examination of the rosette galls revealed that each

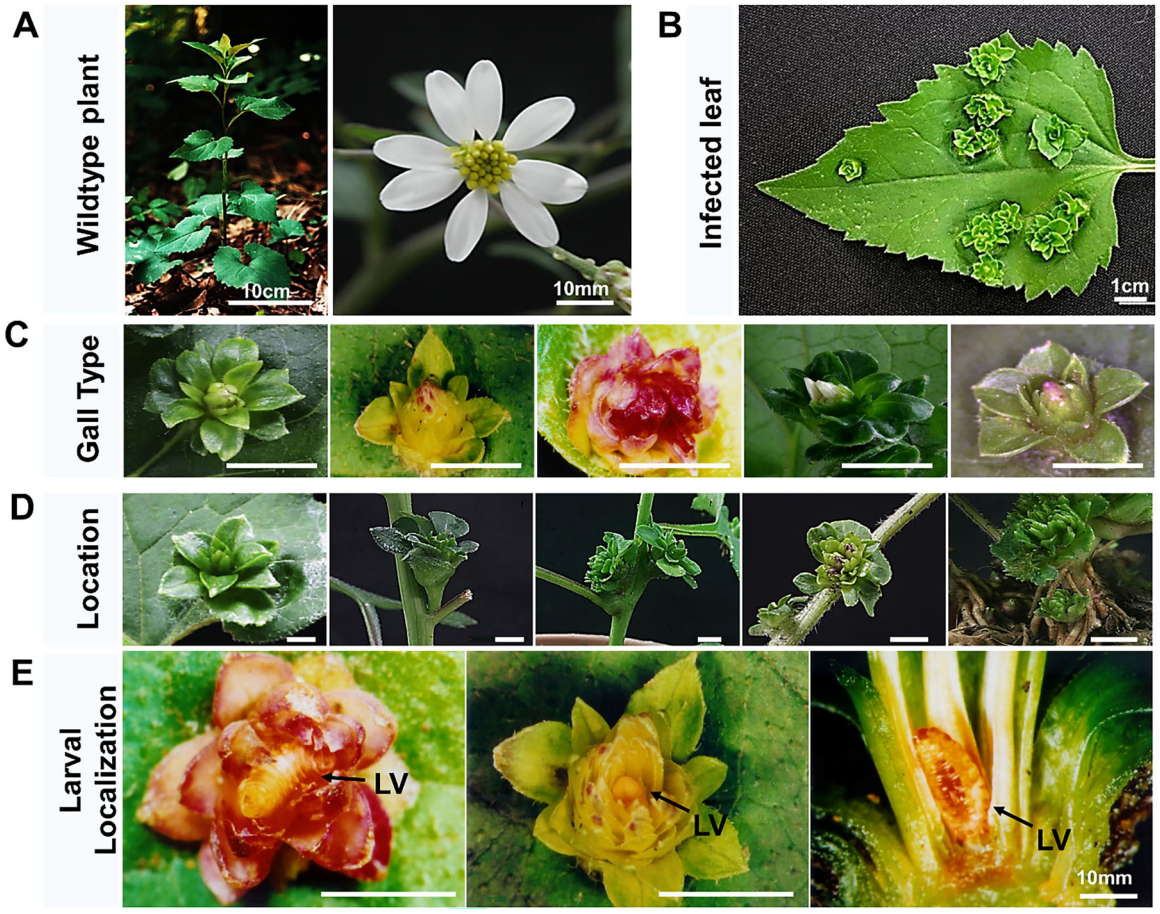

FIGURE 1 | Larvae craft intricate insect rosette galls resembling common flowers. (A) Wild-type plant of *Aster scaber*. Adult plant (left panel) and typical flower (right panel). (B) Infected leaf of *A. scaber*. (C) Gall types of *A. scaber* classified by color, green whorled leaflet only (first panel), green with yellow whorled leaflet (second panel), green with red whorled leaflet (third panel), green with white whorled leaflet (fourth panel), and green with pink whorled leaflet (fifth panel). (D) Various location of galls appearing on leaves (first panel), on stem (two–fourth panel), and on roots (fifth panel) of *A. scaber*. (E) Larvae residing in red (first panel) and in yellow galls (second panel); the vertical section (third panel) shows the larval chamber located within the inner whorled leaflets. LV indicates larvae. All scale bars represent 0.5 cm unless otherwise noted.

gall contained a larva in its inner whorl (Figure 1E). This consistent presence of larvae strongly suggests that these galls were induced by insects. These galls were formed by *D. asteriae* laying eggs on the leaf, stem, and root of *A. scaber* immediately after mating (Figure 2A). Hatched larvae are generally 100–200 μm long and dark orange in color (Figure 2B). The young larvae position themselves vertically and embed into the host plant's organs (Figure 2B). As this occurs, the number of trichomes increases and bends toward the point of embedding, concealing the larva (Figure 2B). Within a week, a dome-like structure appears (Figure 2C), initiating the development of tepal-like leaflets (Figure 2C). These leaflets continue to grow and expand, and begin to produce inner leaflets resembling rosette galls (Figure 2C).

3.2 | Morphological Analysis of Rosette Galls

To study insect-induced rosette gall morphology in detail, we performed histological and electron microscopic analyses of samples from three developmental stages. Rosette galls were categorized into these stages based on their diameter: early stage (approximately 7 mm), middle stage (approximately 10 mm), and late stage (greater than 10 mm). In the early stage, larvae sat in a small chamber surrounded by partly overlapping whorls of tepal-like primordia. Embedded larvae were less than 200 μM long and covered by two tepal-like whorled leaflets (Figure 3A). Horizontal and vertical sections showed that the larvae sat in the center of the whorled leaflets (Figure 3A). SEM analysis showed that the leaflets of whorls simultaneously protruded from galls and gradually expanded in the early stages (Figure 3A). In the middle stage, lateral tepal-like leaflets continued to increase in number from the inner whorls of leaflets and grew perpendicularly to the chamber. Multiple layers of inner tepal-like whorled leaflets fully enclosed the insect-induced meristem-like structure (Figure 3A). Larvae sat in a small chamber surrounded by young leaflet structures exhibiting tepal-like morphology. SEM analysis showed that the concentric leaflet whorls simultaneously further expanded in the middle stages (Figure 3A). In the late stage, lateral tepal-like leaflets continued to increase in number from the inner whorls of leaflets and grew perpendicularly to the chamber. Multiple layers of inner tepal-like whorled leaflets fully enclosed the insect-induced meristem-like structure, while the outer two tepal-like whorled leaflets opened (Figure 3A). Some inner tepal-like whorled leaflets accumulated pigments and lost trichomes, giving them an appearance distinct from typical rosette galls. Moreover, these results suggest that the insect-induced

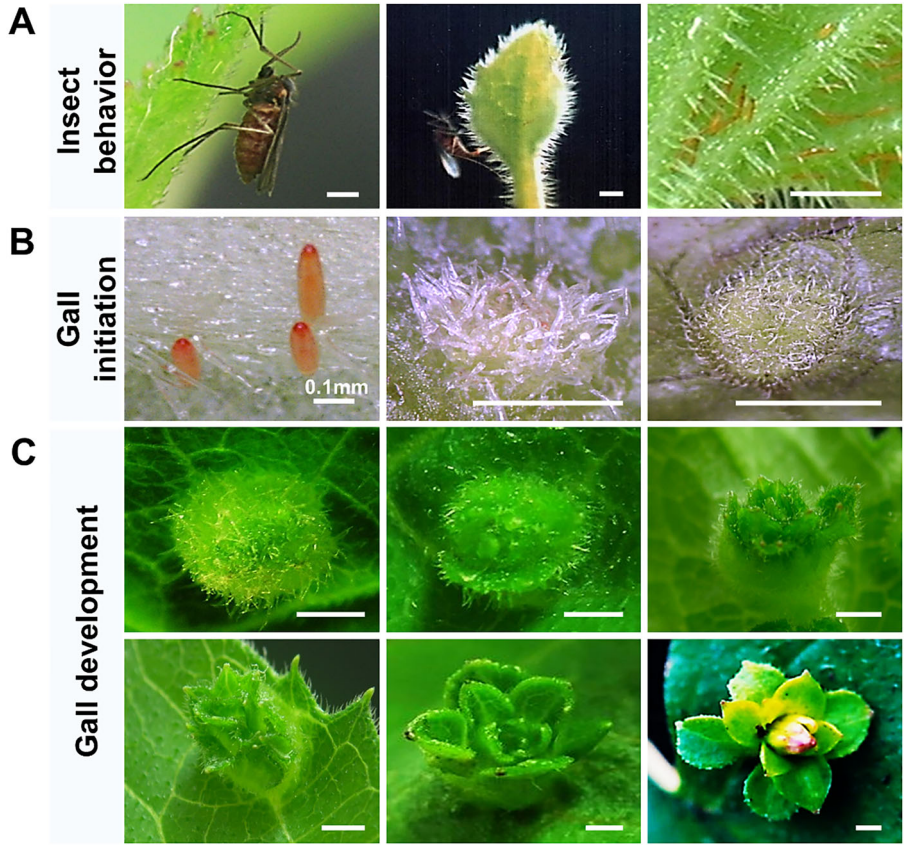

FIGURE 2 | *Dasineura asteriae* larvae systemically modulate gall development. (A) Insect (*D. asteriae*) behavior for gall formation; insect sits on the leaf of *A. scaber* after mating (first panel); insect lays eggs on the leaf (second panel); the eggs of *D. asteriae* are dispersed on the leaf (third panel). (B) Hatched larvae stand upside down and embed their mouth on the leaf, initiating gall formation (first panel); trichomes around the larval site grow to cover the larvae (second panel); the larval embedded site swells up and becomes a dome- shaped gall (third panel). (C) Sepaloid tips extrude from the dome of the gall (top left and middle panel); the tips of sepaloids grow to be two to three whorls (top right panel); sepaloids in the outmost whorls start to open outward and become a rosette gall (bottom left panel); the rosette gall takes shape of gall (bottom middle panel); gall forms pigmented petaloids in the innermost whorls (bottom right panel). All scale bars represent 0.1 cm unless otherwise noted. [Color figure can be viewed at wileyonlinelibrary.com]

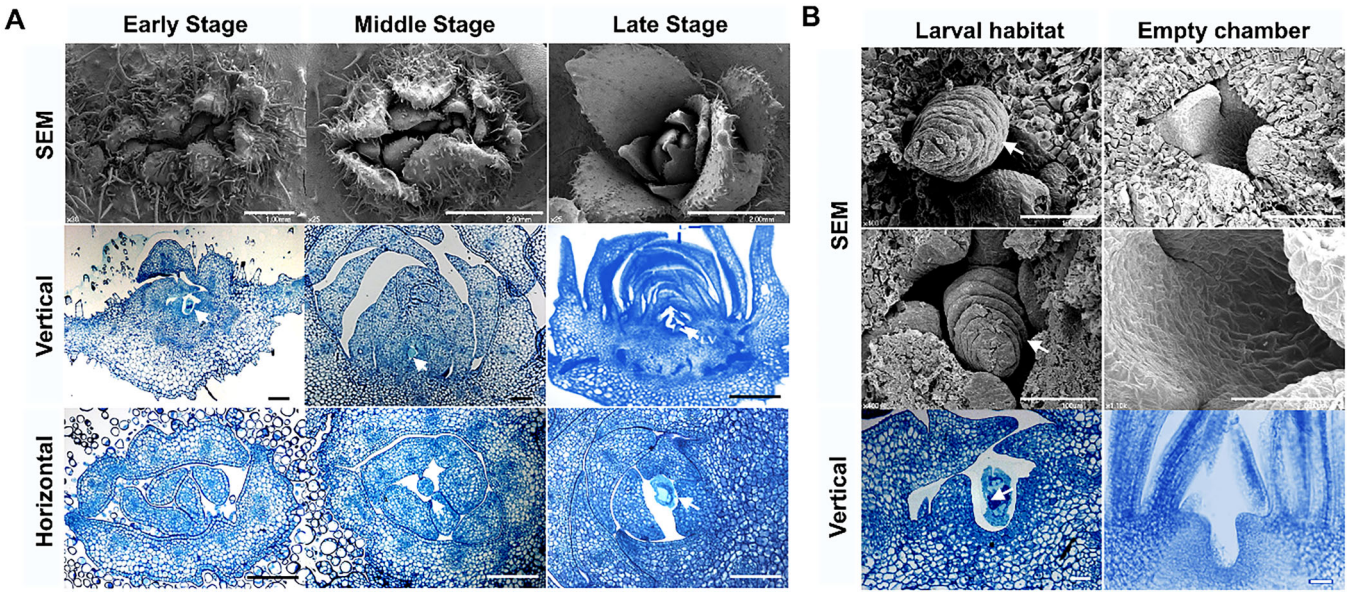

FIGURE 3 | Galls consist of multi-whorled tepal-like leaflets. (A) SEM images of gall surfaces (top row) and sectioned gall tissues at different developmental stage (middle and bottom row). White arrows indicate the larva. (B) Images of the larval habitats within the galls and the empty larval chamber after emergence. SEM images are shown in the first two rows; magnified vertical sections are shown in the bottom row. All scale bars represent 0.1 mm unless otherwise noted. [Color figure can be viewed at wileyonlinelibrary.com]

structure is not merely a consequence of growth disruption but rather an actively organized developmental process resembling aspects of floral meristem initiation. However, we could not find any sign of petal or stamen primordial growth in the early and even middle stages of gall development. Similarly, structures corresponding to reproductive organs were absent, implying that galls consist of only multiple layers of organs mimicking outer floral organs. In place of androecium and gynoecium found in fertile flowers, a central chamber serves as a larval refuge in galls (Figure 3B). The chamber did not expand with larval growth, suggesting that, in the late stage, it may function more as an exit or feeding site rather than a refuge (Figure 3B).

Next, to investigate the morphological characteristics of rosette gall tissue in *A. scaber*, we compared the cell morphology of gall tissues with that of normal leaf tissues (Supporting Information S1: Figure S2A,B). In galls, the round-shaped epidermal cells on the adaxial surface of leaves are transformed into rod-shaped epidermal cells (Supporting Information S1: Figure S2A). The epidermal cells of *A. scaber* leaves typically exhibit trichomes on their surface, however, trichome structures were absent in the gall tissues derived from these leaves. Additionally, the cell morphology in galls gradually transitions from the second whorl to the innermost whorl (Supporting Information S1: Figure S2A). The transition from leaf identity was also indicated by the absence of stomata on the adaxial side of gall organs (Supporting Information S1: Figure S2), distinct from the regular leaf epidermal cells, indicating no apparent morphological similarity between leaf and gall cells (Supporting Information S1: Figure S2A,B).

To further assess the degree of morphological resemblance between the galls and floral structures, we performed SEM imaging with *C. morifolium* (Supporting Information S1: Figure S2C), a representative member of the Asteraceae family known for its characteristic floral architecture. *C. morifolium* flowers are composed of ray and disc florets and are subtended by involucral bracts rather than sepals. Comparative SEM analyses between the rosette galls of *A. scaber* and *C. morifolium* floret revealed notable structural similarities, while no similarities was observed in leaf and involucral bract (Supporting Information S1: Figure S2A,C). suggesting that the insect-induced galls share key morphological features with Asteraceae floral organs. Therefore, these observations indicate that galls likely originate from leaf-derived structures, although the innermost whorls partly imitate petals of Asteraceae, possibly enhancing the resemblance to real flowers and concealing larval chambers.

3.3 | Assembly of Genome and Transcriptome Allowed for Gene Expression Analysis

We initially estimated the genome size of *A. scaber* using two methods, flow cytometry and k-mer spectrum analysis from the generated Illumina gDNA library. Both methods agreed on a haploid genome size of roughly 6 Gb (Supporting Information S1: Figure S3). To further characterize the genome, we generated 367 Gb (62× coverage) of Oxford Nanopore Technologies (ONT) long-read data and 770 Gb (128× coverage) of Illumina short-read data. ONT reads were assembled into an initial assembly of 49 353 contigs with SMARTdenovo (Liu et al. 2021). Furthermore, the assembly was refined by long-read polishing, short-read polishing and finally by removing haplotigs. This resulted in a final assembly of size 4.59 Gb, consisting of 34 571 contigs, with an N50 value of 206.8 kb and a BUSCO completeness score of 86% (Figure 4A).

In parallel, due to the extreme difficulty of assembling a reference-grade 6 Gb genome, we also assembled a reference-grade transcriptome of *A. scaber*, from six RNA-seq libraries of a

wild-type individual (Figure 4B). Consisting of 127,455 transcripts, this assembly has a BUSCO score of 94.1%, showing a near-complete gene content. Because of higher completeness, we used the transcriptome assembly for downstream gene finding and gene expression analyses. To define the corresponding orthologs of *A. thaliana* flowering genes, we employed a comparative genomics approach. We performed gene family analysis with protein sequences of *A. thaliana*, *A. scaber*, and three Asteraceae species with available genome assemblies: *C. cardunculus, C. morifolium* and *H. annuus*. We examined a subset of flowering-related genes, which are selected as the subset of flowering-related genes based on previous reports (Bowman and Moyroud 2024), including *LEAFY* (*LFY*), *APETALA1* (*AP1*), and *AGAMOUS* (*AG*) (Figure 4C). From this clustering of orthologous genes, we defined the *A. scaber* genes of interest. To identify up- and downregulated genes during the gall development, we sequenced the transcriptomes of pairs of galls/uninfected leaves across three stages of the gall (Figure 4D). In the gall, 960, 956, and 1208 genes were upregulated in the early, middle and late stages, respectively (Figure 4E). Only 223 were commonly upregulated in all three stages (Figure 4E). 2112, 1650, and 896 genes, respectively, were downregulated in early, middle, and late stages (Figure 4E). Notably, the middle phase shares more up-and downregulated genes with the early stage than with the late stage (407 and 833 vs. 226 and 272 respectively) indicating that the transcriptome of the fully developed gall is distinct from the earlier stages. The annotated genes in *A. scaber* were comparatively analyzed with those of *A. thaliana*, *C. cardunculus*, *C. morifolium*, and *H. annuus*. The analysis revealed that 10 731 gene families are shared among all five species. Among them, *C. morifolium* exhibited the highest number of unique gene families (8406), followed by *A. scaber*, which possessed 2844 unique gene families (Figure 4F).

3.4 | Flower Development Genes Orchestrate Gall Development

Based on the observation that some gall-derived leaflets exhibit morphology reminiscent of sepals and petals, we next investigated whether this resemblance reflects an underlying

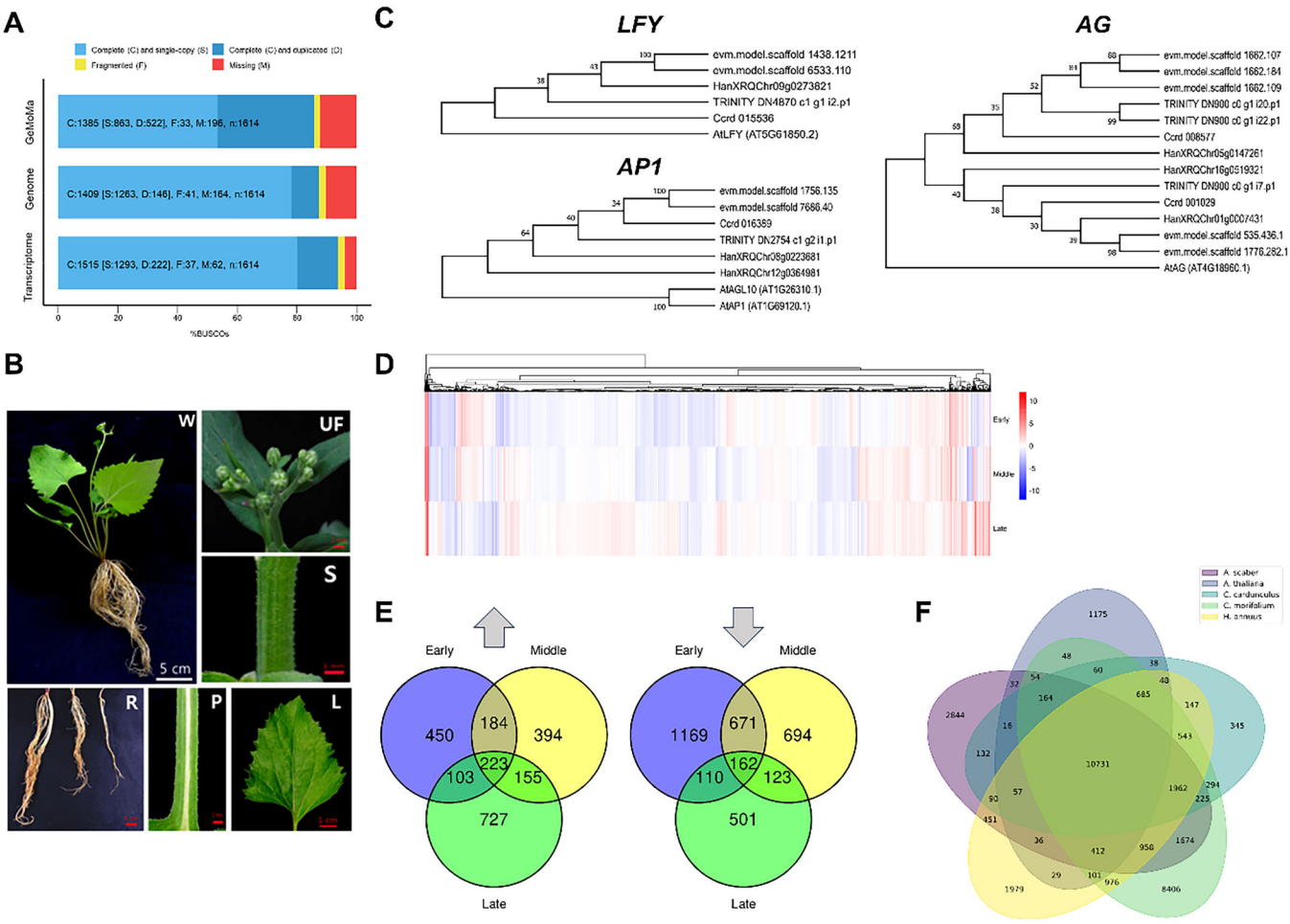

FIGURE 4 | Comprehensive bioinformatic analysis of gene expression and annotation. (A) Gene-completeness assessment of gene annotation, genome assembly, and transcriptome. (B) Tissues used for RNA-seq and transcriptome assembly. (C) Phylogenetic tree of *LFY*, *AP1*, and *AG* orthologs. Numbers at the nodes indicate the branch support, estimated by bootstrapping with 200 replications. (D) Heatmap showing log2 fold-change values of gene TMM values between ectopic shoot and mother leaf, across early, middle, and flowering stages for all genes. (E) Distinct and common upregulated genes and downregulated genes. (F) Gene family analysis reveals distinct and common gene families. Proteomes of *A. scaber*, *Arabidopsis thaliana*, *Chrysanthemum morifolium*, *Helianthus annuus*, and *Cynara cardunculus* were used. [Color figure can be viewed at wileyonlinelibrary.com]

reprogramming of floral regulatory networks. To this end, we examined the expression of genes involved in floral induction and organ specification (Alvarez-Buylla et al. 2010; Espinosa-Soto et al. 2004) from *A. scaber* (Figure 5A) and *C. morifolium* (Figure 5B). Based on *C. morifolium* gene expression data accessed at the Chrysanthemum Genome Database (Ye et al. 2024), we generated a heatmap of ABCE and non-ABCE genes in leaf and various flowering stages (Supporting Information S1: Figure S4A). The genes were defined by the OrthoFinder analysis (Figure 4F) and correspond to genes previously identified (Song et al. 2023). For gall analysis, we utilized dd-PCR due to limited tissue availability, which allowed precise quantification of gene expression (Supporting Information S1: Figure S4B). To confirm the transcriptome patterns, we performed qRT-PCR to analyze the expression levels of ABCE and non-ABCE genes in *C. morifolium* (Figure 5C–H) as well as in *A. scaber* flowers and rosette galls, in a stage-dependent manner. While transcriptome and qRT-PCR analyses revealed some similarities in the expression of key ABCE genes between *C. morifolium* and the rosette galls of *A. scaber*, the expression patterns of non-ABC genes and *AG* differed considerably. In detail, sepals and petals were identified in part by the class A genes *AP1* and *APETALA2* (*AP2*). *AP1* was highly upregulated across all tested stages in the flower and bract of *C. morifolium*, as well as in the flower of *A. scaber* and all three stages of galls (Figure 5C). In contrast, the two *AP2*

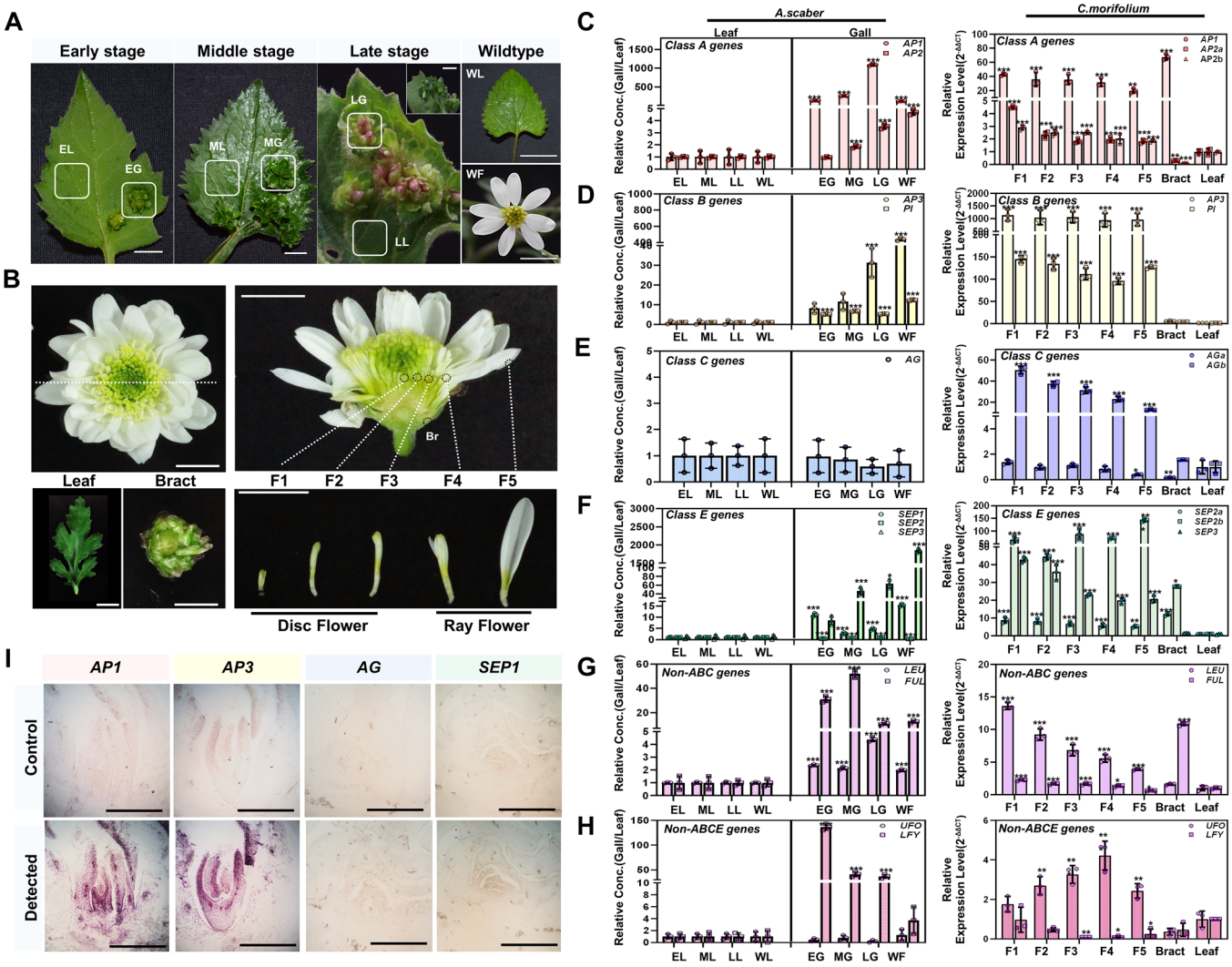

FIGURE 5 | Systemic regulation of floral organogenesis and gene regulatory networks. (A) Samples from *A. scaber*. Galls and corresponding control leaf tissues were collected at three developmental stages; early leaf (EL), early gall (EG), middle leaf (ML), middle gall (MG), late leaf (LL), and late gall (LG). In addition, noninfected wild-type leaf (WL) and wild-type *A. scaber* flower (WF) were included. White boxes indicate gall and control leaf samples used for comparison. Scale bar represents 10 mm. (B) Samples from *C. morifolium*. Flowers, involucral bract and leaf tissues were collected in *C. morifolium*. For flower, samples were collected according to five developmental stages; disc flower [F1 (2–5 mm), F2 (5–8 mm), F3 (8–10 mm)], and ray flower [F4 (8–10 mm), F5 (10 mm ≤)]. Scale bar represents 10 mm. (C–H) Relative expression levels of flowering-related genes categorized by functional class, in *A. scaber* (left) and *C. morifolium* (right). (C) Class A genes (*AP1* and *AP2* in *A. scaber; AP1* and *AP2a/b* in *C. morifolium*). (D) Class B genes (*AP3* and *PI* in both *A. scaber* and *C. morifolium*). (E) Class C genes (*AG* in *A. scaber; AGa/b* in *C. morifolium*). (F) Class E genes (*SEP1*, *SEP2*, and *SEP3* in *A. scaber; SEP2a/b* and *SEP3* in *C. morifolium*) (G, H) Non-ABCE genes in both *A. scaber* and *C. morifolium*. (G) *LEU* and *FUL* genes. (H) *UFO* and *LFY* genes. (I) In situ images showing spatial expression patterns of selected flowering-related genes (*AP1*, *AP3*, *AG* and *SEP1*). Scale bar represent 0.5 mm. [Color figure can be viewed at wileyonlinelibrary.com]

paralogues were upregulated in the flower of *C. morifolium*, but not in the bract. In *A. scaber*, *AP2* expression gradually increased in the galls in a stage-dependent manner and was also elevated in the genuine flower (Figure 5C). Notably, both AP1 and AP2 genes were barely expressed in the leaf controls of *C. morifolium* and *A. scaber*. Given that the basal expression ratio of *AP2* to *AP1* is much higher in *A. scaber* flowers, the elevated *AP2* expression observed in the late stages of gall development may mimic an intrinsic feature of flower development in *A. scaber* (Figure 5C). Petals and stamens in flowers are specified in part by the class B genes *APETALA3* (*AP3*) and *PISTILLATA* (*PI*). Transcript levels of the class B genes, *AP3* and *PI*, were upregulated in *C. morifolium* flowers, *A. scaber* flower, galls, but not in *C. morifolium* bract and the leaf controls of both plants (Figure 5D). Notably, *AP3* expression progressively increased as gall development advanced. In *C. morifolium* bract, class B gene levels were nearly equal to its leaf (Figure 5D). Stamens and carpels are specified in part by the class C gene *AG*. The transcript levels of *AG*, particularly the *AGb* paralogue, were markedly upregulated in *C. morifolium* flowers. In contrast, the orthologous *AG* gene in galls and *A. scaber* flowers was not highly expressed compared to the control leaves (Figure 5E). ABC genes interact with class E genes to form flower organs. The transcript levels of class E genes, *SEPALLATAs* (*SEPs*), were highly upregulated in *C. morifolium* flowers compared to the control leaves (Figure 5F). In contrast, the orthologue of *SEP1* in galls was not highly expressed during early and middle stages, compared to *A. scaber* flowers. As for *SEP2*, neither galls nor *A. scaber* flowers showed significant expression (Figure 5F). To summarize, in the galls of *A. scaber*, all tested ABCE genes, except *AG* and *SEP2*, were upregulated similarly to those in *C. morifolium* flowers (Figure 5C–F). Furthermore, the transcript levels of ABC orthologs in galls showed a profile similar to that observed in *C. morifolium* flowers. Next, we analyzed the transcript levels of non-ABC gene regulators. In *A. thaliana*, *LEUNIG* (*LEU)* acts as a transcriptional co-repressor that interacts with other transcription factors, such as MADS-box proteins, to regulate floral organ identity, especially represses inappropriate expression of class C genes like *AG*. *FRUITFULL* (*FUL*) is a MADS-box transcription factor in *A. thaliana* that regulates fruit development and floral organ growth and contributes to flowering transition (Ó'Maoiléidigh et al. 2014). The transcript levels of *LEU* were upregulated at all stages of gall development and in *A. scaber* flowers compared to control leaves, whereas in *C. morifolium* flowers, *LEU* was highly upregulated at the early stage but gradually decreased thereafter (Figure 5G). Notably, *LEU* orthologue expression was highly upregulated in late stages of galls in contrast to the *A. scaber* flower, suggesting a possible suppression of class C genes (Figure 5G). The transcript levels of *FUL* were highly upregulated in *C. morifolium* bract, but is not upregulated in *C. morifolium* flower. Besides, *FUL* transcripts were notably upregulated in *A. scaber* flowers, and all the tested stage of galls (Figure 5G). *UNUSUAL FLORAL ORGANS* (*UFO*) encodes an F-box protein that acts as a co-factor with *LFY*, a key floral meristem identity gene, to regulate the expression of class B floral homeotic gene *AP3*. *LFY* is a positive regulator of *AP1* and is also involved in lateral flower primordia forming at inflorescence SAM (Samach et al. 1999). In galls, *UFO* was not expressed at any of the tested stages, while *LFY* was highly upregulated at the early stage and gradually decreased through the middle and late stages. Similarly, only *LFY* was notably upregulated in *A. scaber* flowers. In contrast, *UFO* was strongly expressed in *C. morifolium* flowers, whereas *LFY* expression remained minimal, similar to that observed in the bract (Figure 5H). We speculate that the contrasting expression patterns of *UFO* and *LFY* may reflect species-specific regulatory characteristics. In addition, in situ hybridization was conducted to monitor spatial expression patterns of *AP1*, *AP3*, *AG* and *SEP1* genes in *A. scaber* galls. *AP1* and *AP3* were highly expressed, while *SEP1* showed mild expression in the inner whorls of stage middle stage galls, and *AG* was not detected, clearly confirming that galls express key flower-development genes, class A and B (Figure 5I). Taken together, we speculate that the high upregulation of *LEU* in galls may repress *AG*, which plays a key role in identifying carpels and stamens in flowers. Additionally, the lower levels of *UFO* in early and middle stages in galls may affect the role of *AP3*, which is critical for stamen development. *LFY*, which is important for the transition from leaf to flower, was highly upregulated in galls. As a result, during gall development, stamen and carpel formation halts, maintaining the flower-like gall or pseudo-flower state.

3.5 | Cytokinin Accumulates in Rosette Galls of *A. scaber*

At the early stage of gall development, we observed proliferative tissue growth with unorganized cellular architecture surrounding the site of larval oviposition (Figure 2B,C). While the precise identity of these early structures remains unclear, they resembled dedifferentiated or reprogrammed tissues commonly observed in wound-induced organogenesis. As the galls progressed, these tissues gradually differentiated into floral-like structures composed of concentric whorls. To understand the hormonal environment associated with this developmental transition and the maintenance of floral-like identity in galls, we analyzed cytokinin and auxin levels across gall developmental stages (Figures 5B and 6A) using UHPLC/TQ-M analysis. Among the five analogs of cytokinin forms (Figure 6B), such as trans-zeatin riboside 7-glucoside (tZ7G), trans-zeatin riboside (tZR), trans-zeatin O-glucoside (tZOG), trans-zeatin riboside 9-glucoside (tZ9G), and trans-zeatin 9-riboside O-glucoside (tZROG), tZROG was significantly accumulated more than two to fourfold in all the tested gall developmental stages compared to the control leaves (Figure 6C). Notably, tZROG accumulated at significantly higher levels in the buds (4-fold) and true flowers (3-fold) of *A. scaber* compared to the control leaves (Figure 6C). Given that tZROG is a storage form of active cytokinin (Zhao et al. 2024), the available cytokinin reservoir is significantly increased in galls, similar to what is observed in buds and flowers (Figure 6C). In contrast, the other two modified cytokinins, tZ7G and tZOG, did not show significant changes in accumulation levels during gall development. tZ9G, an irreversible and inactive form of cytokinin targeted for degradation, increased during gall development compared to uninfected leaf controls; however, its concentration remained much lower than that of tZOR and tZROG (Figure 6C). The transport form of cytokinin, tZR, was significantly accumulated in the early and middle stages of galls (19-fold and 7-fold, respectively), buds (2-fold), and flower (10-fold) compared to the control leaves (Figure 6C). In the late stage of gall development, tZR levels were about 70% of those in

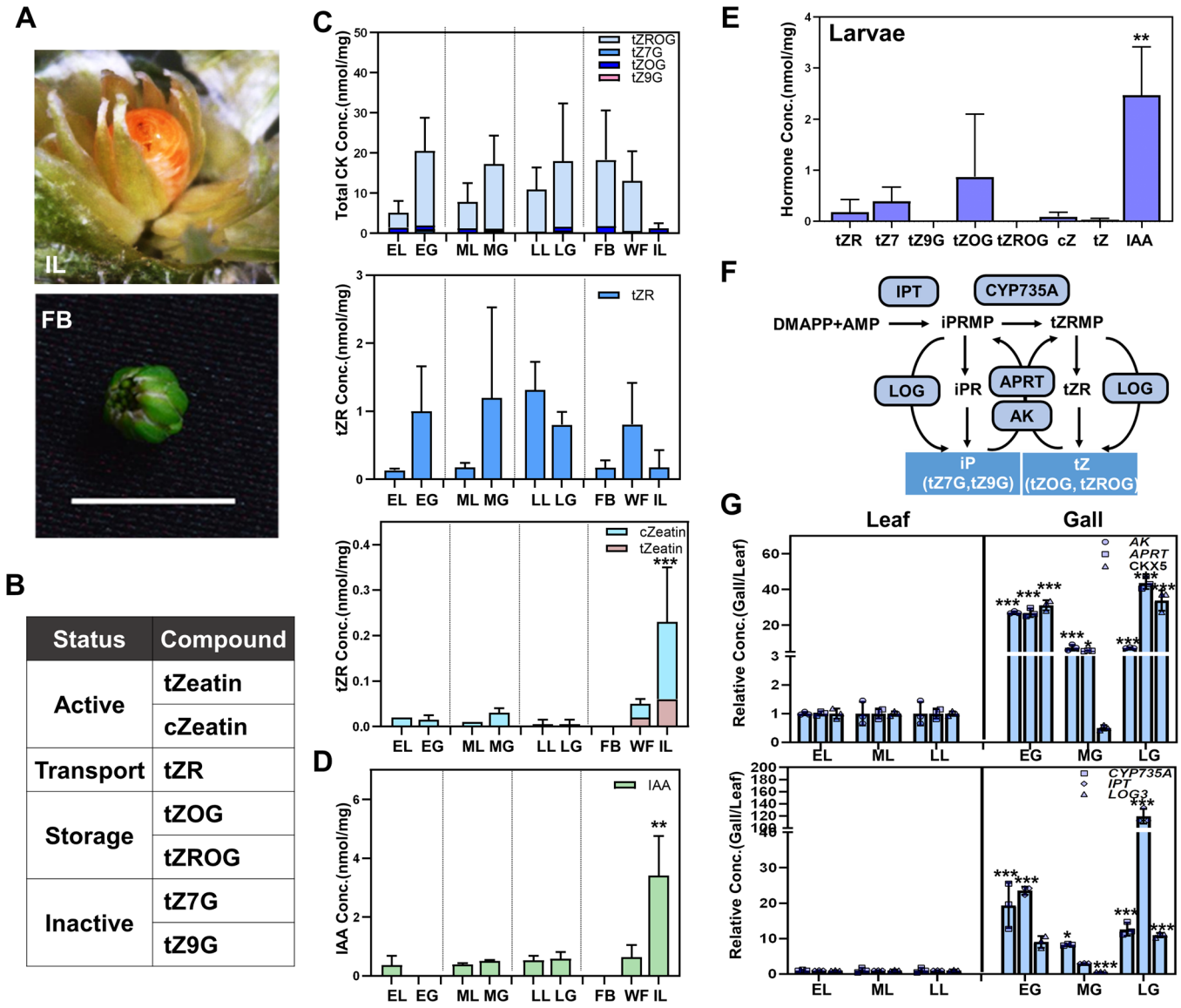

Status	Compound
Active	tZeatin
	cZeatin
Transport	tZR
Storage	tZOG
	tZROG
Inactive	tZ7G
	tZ9G

FIGURE 6 | Cytokinin levels in *A. scaber* insect gall. (A) Additional samples used for cytokinin analysis, including insect larvae (IL) and floral bud (FB), along with the samples described in Figure 5A. Scale bar represent 10 mm. (B) Table listing cytokinin compounds and their abundance status. (C) Cytokinin level in *A. scaber* tissue in three different stages. (D) Paralogue of auxin hormone level in *A. scaber* tissue in three different stages. (E) Paralogue of cytokinin hormone level in larvae. (F) Cytokinin biosynthesis pathway. (G) Transcript level of cytokinin biosynthesis gene performed by Real time PCR. Upper panel shows transcript level of *AK*, *APRT* and *CHX5*, while lower panel shows transcript level of *CYP735A*, *IPT* and *LOG3*. [Color figure can be viewed at wileyonlinelibrary.com]

the surrounding uninfected leaves, suggesting that tZR may have spread from the gall to the nearby leaf tissue. We also monitored the levels of trans-zeatin and cis-zeatin. The former is a biologically active cytokinin, playing key roles in cell division, delaying senescence, and promoting shoot formation, while the latter is an isomer with lower biological activity but specific functions (Schäfer et al. 2015). Unexpectedly, we found that trans-zeatin was almost undetectable during the gall development, and cis-zeatin levels were similar to those of control leaves. Besides, a traceable amount of trans-zeatin, nearly equal to that of cis-zeatin, was detected in the true flowers (Figure 6C). Indole-3-acetic acid (IAA), the most common and biologically active form of auxin, plays a critical role in regulating plant growth and development. During the middle and late stages of gall development, IAA levels were similar to those in the control leaves, except at the early stage (Figure 6D). While exogenous application of intermediate cytokinin-to-auxin ratios is known to promote callus formation under in vitro conditions (Skoog and Miller 1957), the hormone ratios observed in rosette galls, particularly the high tZROG-to-IAA ratio, suggest a distinct hormonal profile more consistent with organized tissue identity than with callus-like proliferation. However, the trans-zeatin and cis-zeatin-to-IAA ratio was exceedingly low, at less than 100-fold, whereas the tZR-to-IAA and tZROG-to-IAA ratios were approximately 3:1 and 36–44:1, respectively. Remarkably, we found that the larvae contained high concentrations of zeatin and auxin (Figure 6C,D). We speculate that these hormones may have been absorbed through sapping, suggesting that the conversion between precursors and zeatin could be active (Figure 6E). Orthologues of cytokinin biosynthesis genes were identified in *A. scaber* (Figure 6F), and transcripts of these genes were upregulated in three different tissues. For example, *ISOPENTENYLTRANSFERASE* (*IPT*), which

regulates the rate-limiting step in cytokinin biosynthesis and *CYTOCHROME P450 MONOOXYGENASE 735A* (*CYP735A*), which is involved in the biosynthesis of phosphorylated N6-isopentenyladenine riboside (iPR) and trans-zeatin were highly upregulated in galls. Additionally, *LONELY GUY 3* (*LOG3*), a cytokinin-activating enzyme that directly activates trans-zeatin, showed significant upregulation in galls (Figure 6G). This is consistent with the high accumulation of tZR and tZROG. In contrast, three negative regulators of cytokinin biosynthesis were also highly upregulated during gall development compared to control leaves; *ADENINE PHOSPHORIBOSYLTRANSFERASE* (*APRT*), which catalyzes the conversion of cytokinin bases to cytokinin nucleotides. *ADENOSINE KINASE* (*AK*), which phosphorylates adenosine (Ado) to AMP, thereby converting iPR monophosphate (iPRMP) from iPR. *CYTOKININ OXIDASE/DEHYDROGENASE 5* (*CKX5*), which catalyzes the degradation of cytokinin (Figure 6G).

4 | Discussion

Our study highlights that *D. asteriae* larvae systemically induce galls that resemble ancestral Asteraceae flowers, which are characterized as pseudoflowers composed of tepaloids. To engineer the development of pseudoflowers, the parasitic larvae selectively activate flower-inducing genes responsible for sepal and petal development, while repressing the class C gene responsible for stamen and carpel formation. Consequently, the floral gene regulatory network is activated in vegetative tissues possibly through the secretion of yet unknown effectors. Unlike normal flowers, which are open structures designed for pollinator visits, rosette galls lack reproductive organs and instead form a closed chamber that protects the larvae.

A. scaber rosette galls exhibit multiple whorls of rosette-shaped tepaloids, whereas *A. scaber* flowers display pappus-like structures, commonly referred to as involucral bracts, characteristic of Asteraceae inflorescences. Unlike the flat, unlayered involucral bracts of *A. scaber* flowers, the gall-derived structures are organized into concentric, pigmented whorls resembling floral perianth organs. Despite these morphological differences, our comparative gene expression analysis reveals notable genetic similarities between *A. scaber* rosette galls and true floral organs. To clarify whether the gall structures can be considered "flower-like", we compared them with *C. morifolium*, a well-characterized member of the Asteraceae, focusing on the expression of key floral identity genes. Notably, qPCR validation revealed that class

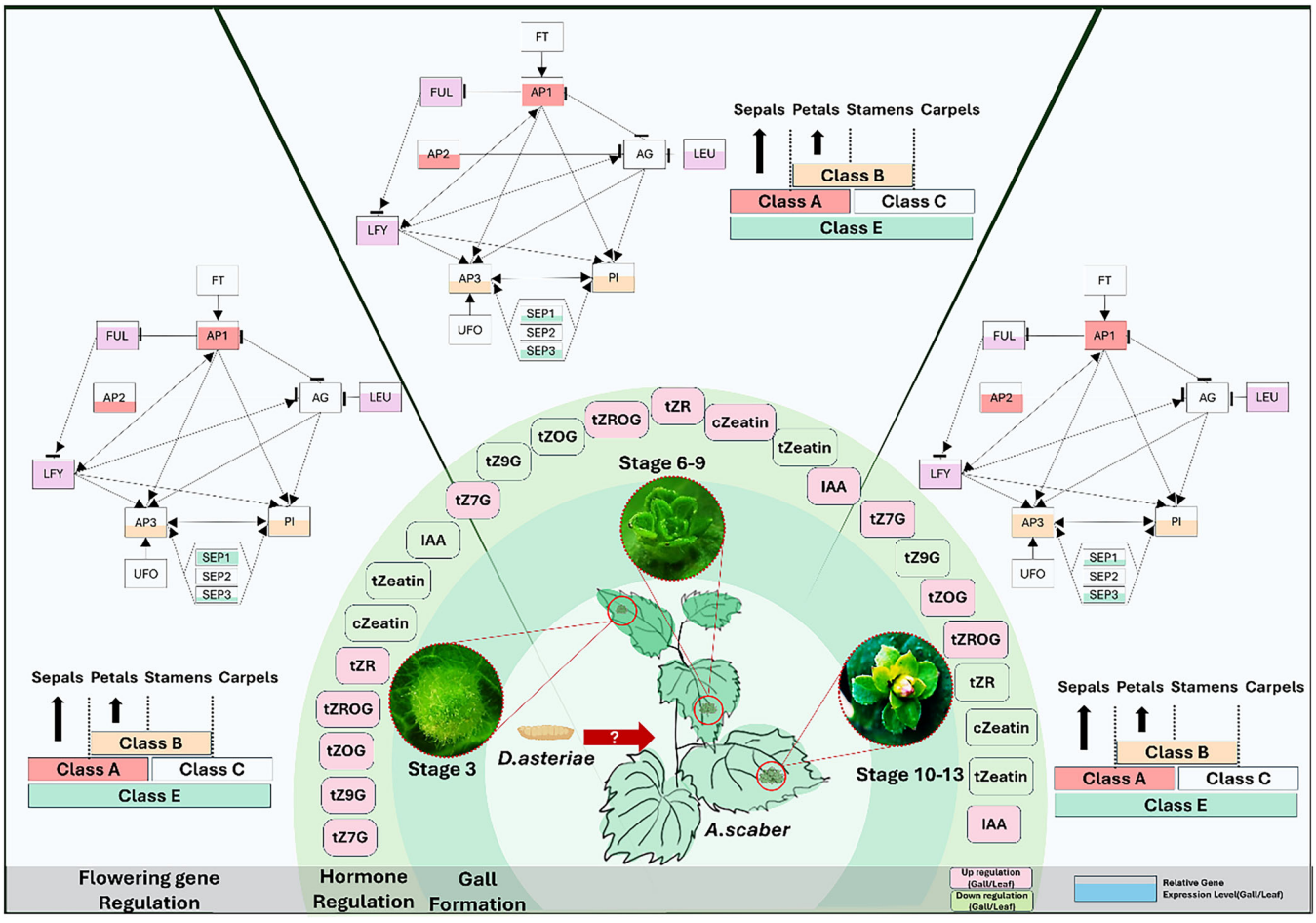

FIGURE 7 | Graphical summary of pseudoflower organogenesis and the associated gene regulatory network. Flower-like gall is induced by unknown elicitors from *D. asteriae* larvae. Throughout pseudoflower development, hormones upregulated compared to leaves are indicated by pink-colored rounded squares, while unaltered hormones are indicated by green-colored rounded squares. Additionally, flowering-related genes show increased expression relative to leaves (color-filled square boxes). Notably, class C genes, which are involved in stamen and carpel development, exhibit minimal expression. In contrast, class A, B and E genes, associated with sepal and petal development, are upregulated. [Color figure can be viewed at wileyonlinelibrary.com]

B genes (*AP3* and *PI*) are absent in *C. morifolium* bracts but are significantly upregulated in the *A. scaber* rosette galls compared to leaf tissues. Taken together, these differences in both gene expression and organ morphology suggest that the gall structures, rather than resembling bracts, exhibit characteristics more reminiscent of petals, such as concentric whorl arrangement, pigmentation, and the upregulation of class B genes, supporting their interpretation as pseudoflowers. This dramatic rewiring of the floral gene network demonstrates how a parasite exploits the inherent plasticity of developmental programs to engineer a novel organ for its benefit.

In response to various biotic stimuli, plants often form unorganized cell masses, such as calluses and tumors. The balance between auxin and cytokinin plays a critical role not only in dedifferentiation and regeneration (Gautheret 1939; Nobécourt 1939; Skoog and Miller 1957; White 1939), but also in broader physiological processes including stress responses and plant-microbe interactions (Großkinsky and Petrášek 2019). Moreover, cytokinin influences floral meristem identity and ovule formation, while auxin regulates petal and carpel outgrowth (Cucinotta et al. 2021). Building on this, we observed that the larvae themselves accumulate high levels of auxin - more than three times that of the *A. scaber* flower – consistent with previous findings in *Pontania* sp. (Yamaguchi et al. 2012). This selective accumulation may contribute to the low auxin levels in the pseudoflower, while storage cytokinin, tZROG, was enriched in the pseudoflowers but absent in *D. asteriae* larvae. One plausible explanation is that auxin is absorbed by the larvae's intestine, while tZROG is excreted into the gall chamber, promoting local cytokinin activity. This could explain why active cytokinin levels appear unchanged, yet functional outcomes such as delayed senescence and callus-like development are evident.

Understanding how the floral gene network contributes to the pseudoflower phenotype also provides insight into its developmental nature. Previous studies of phyllody caused by phytoplasma infection show suppression of floral identity genes and reactivation of vegetative programs (Kitazawa et al. 2017). In contrast, pseudoflowers represent a distinct biotic interaction wherein floral programs are actively promoted. For example, SAP54/PHYL1 effectors downregulate ABCE model genes (Aurin et al. 2020; Maejima et al. 2014; Maejima et al. 2015), while activating *KNOTTED1-LIKE HOMEOBOX* (*KNOX*) and *ASYMMETRIC LEAVES1* (*AS1*) to produce leaf-like organs (Liu et al. 2014), and misregulation of *WUSCHEL* (*WUS*) alters meristem behavior (Wei et al. 2013). Consistently, the transcriptomic analysis revealed that insect-induced pseudoflowers exhibit significant upregulation of key flowering genes, including *AP3*, *PI*, *SEP1*, *SEP3*, *LFY*, and *FUL*, while *AG*, *SEP2*, and *UFO* were not detected (Figure 5D-H). The absence of *AG* likely explains the lack of reproductive organ development, consistent with the low auxin accumulation in pseudoflowers. These changes demonstrate that both structural and molecular floral features can be reprogrammed by parasitic signals.

Taken together, our study uncovers an unusual developmental pathway in which differentiated organs of the host are reprogrammed and subsequently redirected into pseudoflower structures (Figure 7). Although genetic manipulation by the parasite is evident, the specific effector(s) responsible remain unknown. These may include peptides, nucleic acids, hormones, or secondary metabolites – offering a wide range of future targets to investigate.

Acknowledgements

This study was supported by the National Research Foundation of Korea (NRF) grant funded by the Korean Ministry of Science and ICT (No. 2017R1A2B4010255) and by Samsung Science and Technology Foundation Project SSTF-BA1801-09 to S.W.Y. and was also supported by the Basic Science Research Program of the NRF funded by the Korean Ministry of Education (2016R1A6A1A03012862) and (2017R1D1A1B03034952) to K.Z.R and S.K., respectively. The "Cooperative Research Program for Agriculture Science & Technology Development (Project No. PJ01319101)" funded by the Korean Rural Development Administration and a grant (715003-07) from the Research Center for Production Management and Technical Development for High Quality Livestock Products through Agriculture, Food and Rural Affairs Research Center Support Program, Ministry of Agriculture, Food and Rural Affairs to K.Z.R. Lastly, this study was supported by the National Sustainability Program I (NPU w, grant number LO1415) funded by the Ministry of Education, Youth, and Sports of the Czech Republic to T.R. F.B. was supported by core funding from GMI. We extend our special thanks to Mr. Hyengryol Gwak for discovering the ectopic host flowers on galls and to Dr. Ma Yan at GMI for providing expert insights on plant galls.

Conflicts of Interest

The authors declare no conflicts of interest.

Data Availability Statement

Nanopore and Illumina genomic DNA sequencing data will be deposited at ENA Accession PRJEB76616. All RNA-seq data will be deposited at ENA Accession PRJEB81412. The genome and transcriptome assemblies will be made available at https://doi.org/10.6084/m9.figshare.27273801.v1.

References

Alvarez-Buylla, E. R., M. Benítez, A. Corvera-Poiré, et al. 2010. "Flower Development." *Arabidopsis Book* 8: e0127.

Aurin, M.-B., M. Haupt, M. Görlach, F. Rümpler, and G. Theißen. 2020. "Structural Requirements of the Phytoplasma Effector Protein sap54 for Causing Homeotic Transformation of Floral Organs." *Molecular Plant-Microbe Interactions®* 33, no. 9: 1129–1141.

Bailey, S., D. M. Percy, C. A. Hefer, and Q. C. B. Cronk. 2015. "The Transcriptional Landscape of Insect Galls: Psyllid (Hemiptera) Gall Formation in Hawaiian *Metrosideros polymorpha* (Myrtaceae)." *BMC Genomics* 16: 943.

Bowman, J. L., and E. Moyroud. 2024. "Reflections on the Abc Model of Flower Development." *Plant Cell* 36, no. 5: 1334–1357.

Chen, H., J. Liu, K. Cui, et al. 2018. "Molecular Mechanisms of Tannin Accumulation in Rhus Galls and Genes Involved in Plant-Insect Interactions." *Scientific Reports* 8, no. 1: 9841.

Chen, M.-S., H.-X. Zhao, Y. C. Zhu, et al. 2008. "Analysis of Transcripts and Proteins Expressed in the Salivary Glands of Hessian Fly (*Mayetiola Destructor*) Larvae." *Journal of Insect Physiology* 54, no. 1: 1–16.

Chen, X., Z. Yang, H. Chen, et al. 2020. "A Complex Nutrient Exchange Between a Gall-Forming Aphid and Its Plant Host." *Frontiers in Plant Science* 11: 811.

Cucinotta, M., A. Cavalleri, J. W. Chandler, and L. Colombo. 2021. "Auxin and Flower Development: A Blossoming Field." *Cold Spring Harbor Perspectives in Biology* 13, no. 2: a039974.

Espinosa-Soto, C., P. Padilla-Longoria, and E. R. Alvarez-Buylla. 2004. "A Gene Regulatory Network Model for Cell-Fate Determination During *Arabidopsis thaliana* Flower Development That Is Robust and Recovers Experimental Gene Expression Profiles." *Plant Cell* 16, no. 11: 2923–2939.

Espírito-Santo, M. M., and G. W. Fernandes. 2007. "How Many Species of Gall-Inducing Insects Are There on Earth, and Where Are They?" *Annals of the Entomological Society of America* 100, no. 2: 95–99.

Flynn, J. M., R. Hubley, C. Goubert, et al. 2020. "Repeatmodeler2 for Automated Genomic Discovery of Transposable Element Families." *Proceedings of the National Academy of Sciences* 117, no. 17: 9451–9457.

Gätjens-Boniche, O., J. P. Jiménez-Madrigal, R. W. Whetten, et al. 2023. "Microbiome and Plant Cell Transformation Trigger Insect Gall Induction in Cassava." *Frontiers in Plant Science* 14: 1237966.

Gautheret, R. 1939. "Sur la possibilité de réaliser la culture indéfinie des tissus de tubercules de carotte." *CR Hebd Seances Acad Sc* 208: 118–120.

Grabherr, M. G., B. J. Haas, M. Yassour, et al. 2011. "Full-Length Transcriptome Assembly From RNA-Seq Data Without a Reference Genome." *Nature Biotechnology* 29, no. 7: 644–652.

Großkinsky, D. K., A. Albacete, A. Jammer, et al. 2014. "A Rapid Phytohormone and Phytoalexin Screening Method for Physiological Phenotyping." *Molecular Plant* 7, no. 6: 1053–1056.

Großkinsky, D. K., and J. Petrášek. 2019. "Auxins and Cytokinins–The Dynamic Duo of Growth-Regulating Phytohormones Heading for New Shores." *New Phytologist* 221, no. 3: 1187–1190.

Hammer, T. J., R. De Clerck-Floate, J. F. Tooker, P. W. Price, D. G. Miller, and E. F. Connor. 2021. "Are Bacterial Symbionts Associated With Gall Induction In Insects?" *Arthropod-Plant Interactions* 15: 1–12.

Hardy, N. B., and L. G. Cook. 2010. "Gall-Induction in Insects: Evolutionary Dead-End or Speciation Driver?" *BMC Evolutionary Biology* 10: 257.

Hu, J., J. Fan, Z. Sun, and S. Liu. 2020. "Nextpolish: A Fast and Efficient Genome Polishing Tool for Long-Read Assembly." *Bioinformatics* 36, no. 7: 2253–2255.

Huang, N., and H. Li. 2023. "Compleasm: A Faster and More Accurate Reimplementation of Busco." *Bioinformatics* 39, no. 10: btad595.

Keilwagen, J., F. Hartung, and J. Grau. 2019. "Gemoma: Homology-Based Gene Prediction Utilizing Intron Position Conservation and RNA-Seq Data." *Gene Prediction: Methods in Molecular Biology (Clifton, N.J.)* 1962: 161–177.

Kitazawa, Y., N. Iwabuchi, M. Himeno, et al. 2017. "Phytoplasma-Conserved Phyllogen Proteins Induce Phyllody Across the Plantae by Degrading Floral Mads Domain Proteins." *Journal of Experimental Botany* 68, no. 11: 2799–2811.

Kokot, M., M. Długosz, and S. Deorowicz. 2017. "Kmc 3: Counting and Manipulating K-Mer Statistics." *Bioinformatics* 33, no. 17: 2759–2761.

Korgaonkar, A., C. Han, A. L. Lemire, et al. 2021. "A Novel Family of Secreted Insect Proteins Linked to Plant Gall Development." *Current Biology* 31, no. 9: 1836–1849.e12.

Labandeira, C. C., and T. L. Phillips. 1996. "A Carboniferous Insect Gall: Insight Into Early Ecologic History of the Holometabola." *Proceedings of the National Academy of Sciences* 93, no. 16: 8470–8474.

Li, W. P., F. S. Yang, T. Jivkova, and G. S. Yin. 2012. "Phylogenetic Relationships and Generic Delimitation of Eurasian Aster (Asteraceae: Astereae) Inferred From its, ets and trnl-f Sequence Data." *Annals of Botany* 109, no. 7: 1341–1357.

Liu, H., S. Wu, A. Li, and J. Ruan. 2021. "Smartdenovo: A De Novo Assembler Using Long Noisy Reads." *Gigabyte* 2021: gigabyte15.

Liu, L.-Y. D., H.-I. Tseng, C.-P. Lin, et al. 2014. "High-Throughput Transcriptome Analysis of the Leafy Flower Transition of *Catharanthus roseus* Induced by Peanut Witches;-Broom Phytoplasma Infection." *Plant and Cell Physiology* 55, no. 5: 942–957.

Liu, X., C. Khajuria, J. Li, et al. 2013. "Wheat mds-1 Encodes a Heat-Shock Protein and Governs Susceptibility Towards the Hessian Fly Gall Midge." *Nature Communications* 4, no. 1: 2070.

Maejima, K., R. Iwai, M. Himeno, et al. 2014. "Recognition of Floral Homeotic Mads Domain Transcription Factors by a Phytoplasmal Effector, Phyllogen, Induces Phyllody." *Plant Journal* 78, no. 4: 541–554.

Maejima, K., Y. Kitazawa, T. Tomomitsu, et al. 2015. "Degradation of Class E Mads-Domain Transcription Factors in Arabidopsis by a Phytoplasmal Effector, Phyllogen." *Plant Signaling & Behavior* 10, no. 8: e1042635.

Markel, K., V. Novak, B. P. Bowen, et al. 2024. "Cynipid Wasps Systematically Reprogram Host Metabolism and Restructure Cell Walls in Developing Galls." *Plant Physiology* 195, no. 1: 698–712.

Murakami, R., R. Ushima, R. Sugimoto, et al. 2021. "A New Galling Insect Model Enhances Photosynthetic Activity In An Obligate Holoparasitic Plant." *Scientific Reports* 11, no. 1: 13013.

Nabity, P. D., M. J. Haus, M. R. Berenbaum, and E. H. DeLucia. 2013. "Leaf-Galling Phylloxera on Grapes Reprograms Host Metabolism and Morphology." *Proceedings of the National Academy of Sciences* 110, no. 41: 16663–16668.

Nesom, G. L. 1994. "A New Species of Lippia (Verbenaceae) From South-Central Mexico, With Comments on Related and Peripheral Species." *Phytologia* 77: 309–317.

Nobécourt, P. 1939. "Sur la pérennité et l'augmentation de volume des cultures de tissues végétaux." *CR Seances Soc Biol Ses Fil* 130: 1270–1271.

Ó'Maoiléidigh, D. S., E. Graciet, and F. Wellmer. 2014. "Gene Networks Controlling a Rabidopsis Thaliana Flower Development." *New Phytologist* 201, no. 1: 16–30.

Oates, C., K. Denby, A. Myburg, B. Slippers, and S. Naidoo. 2016. "Insect Gallers and Their Plant Hosts: From Omics Data to Systems Biology." *International Journal of Molecular Sciences* 17, no. 11: 1891.

Oliveira, D. C., R. M. S. Isaias, G. W. Fernandes, B. G. Ferreira, R. G. S. Carneiro, and L. Fuzaro. 2016. "Manipulation of Host Plant Cells and Tissues by Gall-Inducing Insects and Adaptive Strategies Used by Different Feeding Guilds." *Journal of Insect Physiology* 84: 103–113.

Paik, J.-C., J. Yukawa, N. Uechi, S. Sato, and T. Ganaha. 2004. "Gall-Inducing Species of the Family Cecidomyiidae (Diptera) Recorded From the Korean Peninsula and Surrounding Islands, in Comparison With the Gall-Midge Fauna of Japan." *ESAKIA* 44: 57–66.

Patro, R., G. Duggal, M. I. Love, R. A. Irizarry, and C. Kingsford. 2017. "Salmon Provides Fast and Bias-Aware Quantification of Transcript Expression." *Nature Methods* 14, no. 4: 417–419.

Price, P. W., G. W. Fernandes, and G. L. Waring. 1987. "Adaptive Nature of Insect Galls." *Environmental Entomology* 16, no. 1: 15–24.

Ranallo-Benavidez, T. R., K. S. Jaron, and M. C. Schatz. 2020. "Genomescope 2.0 and Smudgeplot for Reference-Free Profiling of Polyploid Genomes." *Nature Communications* 11: 1432.

Roach, M. J., S. A. Schmidt, and A. R. Borneman. 2018. "Purge Haplotigs: Allelic Contig Reassignment for Third-Gen Diploid Genome Assemblies." *BMC Bioinformatics* 19: 460.

Samach, A., J. E. Klenz, S. E. Kohalmi, E. Risseeuw, G. W. Haughn, and W. L. Crosby. 1999. "The Unusual Floral Organs Gene of *Arabidopsis thaliana* Is an F-Box Protein Required for Normal Patterning and Growth In the Floral Meristem." *Plant Journal* 20, no. 4: 433–445.

Schäfer, M., C. Brütting, I. D. Meza-Canales, et al. 2015. "The Role of Cis-Zeatin-Type Cytokinins in Plant Growth Regulation and Mediating Responses to Environmental Interactions." *Journal of Experimental Botany* 66, no. 16: 4873–4884.

Schultz, J. C., P. P. Edger, M. J. A. Body, and H. M. Appel. 2019. "A Galling Insect Activates Plant Reproductive Programs During Gall Development." *Scientific Reports* 9, no. 1: 1833.

Shinji, O. 1944. Chuei to chuei konchu: Galls and Gall Making Insects, 580.

Sinha, D. K., J. Nagaraju, A. Tomar, J. S. Bentur, and S. Nair. 2012. "Pyrosequencing-Based Transcriptome Analysis of the Asian Rice Gall Midge Reveals Differential Response During Compatible and Incompatible Interaction." *International Journal of Molecular Sciences* 13, no. 10: 13079–13103.

Skoog, F., and C. O. Miller. 1957. "Chemical Regulation of Growth and Organ Formation in Plant Tissues Cultured In Vitro." *Symposia of the Society for Experimental Biology* 11: 118–130.

Song, A., J. Su, H. Wang, et al. 2023. "Analyses of a Chromosome-Scale Genome Assembly Reveal the Origin and Evolution of Cultivated Chrysanthemum." *Nature Communications* 14, no. 1: 2021.

Stern, D. L., and C. Han. 2022. "Gene Structure-Based Homology Search Identifies Highly Divergent Putative Effector Gene Family." *Genome Biology and Evolution* 14, no. 6: evac069.

Stone, G. N., and K. Schönrogge. 2003. "The Adaptive Significance of Insect Gall Morphology." *Trends in Ecology & Evolution* 18, no. 10: 512–522.

Tokuda, M., J. Yukawa, V. N. Kuzntsov, and A. E. Kozhevnikov 2003. Asteralobia Gall Midges (diptera: Cecidomyiidae) on Aster Species (asteraceae) in Japan and the Russian Far East.

Wei, H. Y., Y. X. Ye, H. J. Huang, et al. 2022. "Chromosome-Level Genome Assembly for the Horned-Gall Aphid Provides Insights into Interactions Between Gall-Making Insect and Its Host Plant." *Ecology and Evolution* 12, no. 4: e8815.

Wei, W., R. E. Davis, D. L. Nuss, and Y. Zhao. 2013. "Phytoplasmal Infection Derails Genetically Preprogrammed Meristem Fate and Alters Plant Architecture." *Proceedings of the National Academy of Sciences* 110, no. 47: 19149–19154.

White, P. R. 1939. "Potentially Unlimited Growth of Excised Plant Callus in an Artificial Nutrient." *American Journal of Botany* 26: 59–64.

Yamaguchi, H., H. Tanaka, M. Hasegawa, M. Tokuda, T. Asami, and Y. Suzuki. 2012. "Phytohormones and Willow Gall Induction by a Gall-Inducing Sawfly." *New Phytologist* 196, no. 2: 586–595.

Ye, J., C. Wang, Y. Liu, et al. 2024. "Cgd: A Multi-Omics Database for Chrysanthemum Genomic and Biological Research." *Horticulture Research* 11, no. 11: uhae238.

Yukawa, J., M. Tokuda, and K. Yamagishi. 2014. "Host Plant Ranges and Distribution Records of Identified and Unidentified Species of the Genus Lasioptera (Diptera: Cecidomyiidae) In Japan." *ESAKIA* 54: 1–15.

Zhang, Z., W. Shi, J. Gu, et al. 2024. "Short Day Promotes Gall Swelling by a Constans-Flowering Locus T Pathway in *Zizania latifolia*." *Plant Journal* 120, no. 3: 1014–1031.

Zhao, C., L. N. Escalante, H. Chen, et al. 2015. "A Massive Expansion of Effector Genes Underlies Gall-Formation in the Wheat Pest *Mayetiola Destructor*." *Current Biology* 25, no. 5: 613–620.

Zhao, C., R. Shukle, L. Navarro-Escalante, M. Chen, S. Richards, and J. J. Stuart. 2016. "Avirulence Gene Mapping in the Hessian Fly (*Mayetiola Destructor*) Reveals a Protein Phosphatase 2c Effector Gene Family." *Journal of Insect Physiology* 84: 22–31.

Zhao, J., J. Wang, J. Liu, et al. 2024. "Spatially Distributed Cytokinins: Metabolism, Signaling, and Transport." *Plant Communications* 5: 100936.

Supporting Information

Additional supporting information can be found online in the Supporting Information section.
Boo et al.